PHYSICAL REVIEW B VOLUME 23, NUMBER 10 15 MAY 1981

New model of nuclear particle tracks in dielectric minerals

E. Dartyge
Laboratoire de Physique du Solide, 91406 Orsay, France

J. P. Duraud
Département de Physico-Chimie, Centre d'Etudes Nucléaires de Saclay, B.P. 2, 91190 Gif-sur-Yvette, France

Y. Langevin and M. Maurette
Laboratoire René-Bernas du Centre de Spectrométrie Nucléaire et de Spectrométrie de Masse, 91406 Orsay, France

(Received 23 July 1980)

The microscopic structure of latent tracks in silicates is analyzed using small-angle x-ray scattering methods. Latent tracks are constituted of extended defects, separated by gap zones loaded with point defects. The variation of the linear density of extended defects along the path of the incident ions cannot be scaled with functions previously used, such as the primary rate of ionization. Upon a thermal annealing, the extended defects are much more stable than point defects. These latent tracks are chemically etched and their etching rates are inferred from optical and scanning electron-microscope observations. From these combined studies of latent and etched tracks, a model for the registration of etchable tracks in silicates is developed. In this model, the extended defects dominate the chemical etching and thermal annealing behavior of etchable tracks. The marked differences observed in the sensitivity of various silicates are no longer attributed to a radiation damage mechanism, which would operate much more efficiently in specific silicates, but to the etching behavior of each mineral. Indeed, for a given incident ion, the linear density of extended defects in a given part of the ion residual range appears to be similar in all silicates. This model is used in the framework of a Monte Carlo statistical code to predict etched track-length distributions in silicates, including those relevant to partially annealed tracks. The striking agreement between these predictions and the corresponding observations strongly support our model. It enables us to discuss the most important concepts previously proposed to account for the registration of etchable tracks in silicates, and to suggest a few preliminary guidelines for improving the use of solid-state track detectors.

I. INTRODUCTION

Heavy ions produce linear trails of damaged material (latent tracks) in dielectric minerals, which can be conveniently observed with an optical microscope after an appropriate chemical etching. Since the pioneering work of Fleischer, Price, and Walker,[1] the study of etchable tracks has provided very valuable results in various fields, such as nuclear physics,[2] cosmic-ray physics,[3] geochronology,[4] and meteoritic and lunar sciences.[5] However, there are still basic limitations in the applications of these studies. This is mostly related to the difficulty encountered in defining the microscopic structure of the latent track,[6] which prevents a good understanding of the basic processes responsible for the chemical etching and the thermal annealing of the latent track. Consequently, important parameters extensively used in track studies, such as the "etchable range" $\Delta R(Z)$ of a given ion, can neither be defined with sufficient accuracy nor be corrected for natural thermal annealing effects as in the case of fossil tracks registered in natural minerals.[7]

This comment is particularly relevant to one of the most exciting applications of etched-track studies in extraterrestrial minerals, namely the determination of the chemical composition of very heavy nuclei in the ancient cosmic rays at known epochs in the distant past.[8] For this purpose, the length distribution of the corresponding fossil tracks is measured. Then, a $\Delta R(Z)$ scaling function determined from calibration experiments is used both to identify various groups of heavy nuclei in the cosmic rays and to relate the density of tracks with a given length to the abundance of the corresponding track-producing nuclei. However, in these studies, the value of $\Delta R(Z)$ was uncertain for the following reasons:

(i) The direct determination of $\Delta R(Z)$ for heavy ions was not possible as the energies reached in available accelerators were too low.

(ii) The "threshold" track-formation mechanism used to define $\Delta R(Z)$ for the unannealed tracks does not well account for experimental results recently reported.[9,10]

(iii) Several groups[7,10,11] have shown that cosmic-ray tracks in extraterrestrial material have been altered as the result of a natural thermal annealing. Consequently, the use of the unannealed $\Delta R(Z)$ scaling function is not appropriate.

In this paper we attempt to improve the reliability of etched-track studies in dielectric minerals by combining small-angle x-ray scattering analysis of the microscopic structure of the latent tracks with the measurement of their etching rates both before and after a thermal annealing. The

tracks were produced by irradiating the external surface of various silicates with parallel beams of heavy ions, with a wide variety of energies and atomic numbers. In Sec. II we summarize our experimental procedure and we show that the external irradiation geometry is the most useful scheme in testing the validity of a track-registration model. In Sec. III we present those of our experimental results that we consider the most critical for such a model. In Sec. IV, we develop a new model for the chemical etching of latent tracks, which enabled us to compute for the first-time track-length distributions.[8] We note that the striking agreement between the theoretical predictions and the corresponding experimental observations strongly supports the validity of our model. We also show in this section how the unique etching properties of muscovite mica together with the x-ray observations allow a determination of the basic parameters of the model, and that these results are not dependent on parameter-fitting techniques. In the last section of this paper we discuss the basic concepts, that have been applied in this paper, to describe the registration of etchable tracks in dielectric minerals. This discussion already provides useful guidelines for a better use of tracks registered in solid-state detectors, which will be developed in a forthcoming paper.

II. EXPERIMENTAL PROCEDURE

A. Samples and irradiation conditions

We selected four silicates (muscovite mica, labradorite, pyroxene, and olivine) that have been widely used in previous studies of fossil tracks in terrestrial and extraterrestrial samples. Muscovite and olivine were also selected on the basis of track-registration studies which rank these two minerals among the most and the least "sensitive," respectively.[12] It was important to check whether or not this observation implied the existence of a threshold track-formation mechanism operating with a greater efficiency in mica.[13] Furthermore, mica and labradorite represent two extreme types of track detectors. Indeed, in mica the perpendicular etching rates, V_{hkl}, of the various crystallographic planes are highly anisotropic, while the V_{hkl} etching rates in labradorite do not differ by more than a factor of two[12] (see Sec. IV for the measurement of V_{hkl}).

After preliminary studies of etched tracks (that confirmed our much earlier conclusions[14]), we decided to reject pyroxene as a reliable track detector because tracks are not homogeneously registered. Also, the x-ray studies were so far limited to mica and olivine because the preparation of the required thin slabs of labradorite is very difficult.

For the x-ray studies, 10-μm-thick lamellae of mica were prepared by cleavage, while a wire saw was used to obtain 30-μm-thick slabs of olivine. The thickness of these thin samples was determined with an accuracy of ~1 μm with an optical microscope. For etched-track studies, much thicker samples were prepared with the same techniques.

These samples were irradiated with Ne, Ar, Fe, Cu, Kr, and Xe ions at several accelerators (CEV Orsay, Tandem Orsay, Linac Manchester, Heavy ion cyclotron, Dubna). The initial energy of the ion could be preset with an accuracy of $\lesssim$1% between a lower limit of ~0.2 MeV/amu and a maximum value of ~10 MeV/amu for Kr ions. For the x-ray analysis, the samples were irradiated with an ion fluence $\gtrsim 10^{11}$ ions cm^{-2}, and the range-energy curves of Henke and Benton[15] were used to evaluate the average ion energy in the samples. For etched-track studies, a rotating diaphragm was used to obtain the much smaller ion fluence required (~10^6 ions cm^{-2}). Ion fluences were determined with an accuracy of $\lesssim$10% by measuring the ion-beam intensity both before and after the irradiation.

We investigated the characteristics of latent and etched tracks both before and after thermal annealing runs conducted in a controlled atmosphere of argon. A series of samples was first annealed at several temperatures up to 900 °C for periods of two hours (isochronal annealings) to identify the critical temperatures at which marked changes in either the latent-track structure or the etched-track-length distributions are observed. Then isothermal annealings at these critical temperatures were conducted to evaluate the kinetics of the annealing process.

The most important applications of etched-track studies deal with a very different irradiation geometry, namely, where the tracks accumulate *within* the volume of their host minerals. In Sec. V we will indicate a few guidelines needed to extrapolate the results of the external track-irradiation geometry reported in this paper to the internal track-irradiation geometry relevant to fossil tracks. We just want to emphasize here that the external track geometry is the best one to check the validity of a track-registration model. In this particular scheme, the tracks produced by a given ion intersect the observation plane at a well-defined value of the ion residual range, R, which can be determined with an accuracy of ~1%. In sharp contrast, internal tracks intersect the observation plane anywhere along their range, and thus the energy of the ions cannot be defined

TABLE I. Notations and symbols.

Z	atomic energy of the incident ion
E	energy of the incident ion
R_0	total range of the incident ion
R	residual range of the incident ion
T	annealing temperature
t, t_0	etching time, standard etching time
Θ, Λ	diffusion angle and wavelength of the x rays
$s, I(s)$	modulus and scattered intensity of the x rays
$\Delta\epsilon_1, \Delta\epsilon_2$	electronic density deficit in point and extended defects
$n(R), N(R)$	linear density of point and extended defects
J	primary ionization rate
ρ	track density
θ	angle between the track and the observation plane
L, L_0	observable and total etched length along the track
Fe(E)	tracks produced by Fe ions with energy E (MeV/amu)
$D_L\{R;(t,T)\}$	length distribution of tracks starting at a residual range R, annealed at the temperature T (2 h), and etched a time t
V_{hkl}, V_0, V_p	etch rates in the direction hkl, along the track, and perpendicular to the observation plane, respectively
$V_g, V_c, V_b(R,T)$	etch rates of gap zones, core zones, and bulk etch rate of the track as a function of the residual range
$\alpha(T)$	scaling factor of track-length distributions after a low-temperature annealing
λ_c	effective length of core zones
d	width of a gap zone
$w(R)$	aggregated width of gap zones per micrometer of range
$N_g(R)$	linear density of gaps per micrometer of range
$\eta(R)$	etching efficiency
ν	volume density of track-forming events
β	minimum depth-diameter ratio below which a track cannot be identified

with any accuracy. Consequently, as shown in Sec. V, there is a considerable spread of the track-etching rate and the track-length distributions, which smears out the intrinsic etching properties of the tracks.

B. X-ray measurements

In our x-ray apparatus which has been described elsewhere,[16] the intensity of the scattered x rays is measured as a function of the angular distance to the center of the diffraction spot. This intensity, $I(s)$, is conveniently expressed in terms of a diffusion vector characterized by a modulus, $s = 2\sin\Theta/\Lambda$, where 2Θ is the diffusion angle and Λ is the wavelength of the monochromatic incident x-ray beam (see Table I).

The resulting signal is interpreted in te ms of point defects and extended defects using mathematical methods extensively discussed elsewhere.[17] The point defects give a diffuse background which is independent of s [Fig. 1(a)], while the characteristic signature of the extended defects is a sharp increase in the value of $I(s)$ with decreasing values of s [Fig. 1(b)]. The mathematical analysis of such signals then yields the size of each type of defects as well as the products $n(R)\Delta\epsilon_1^2$ and $N(R)\Delta\epsilon_2^2$ as a function of the residual range R of the incident ions. $\Delta\epsilon_1$ and $\Delta\epsilon_2$ repre-

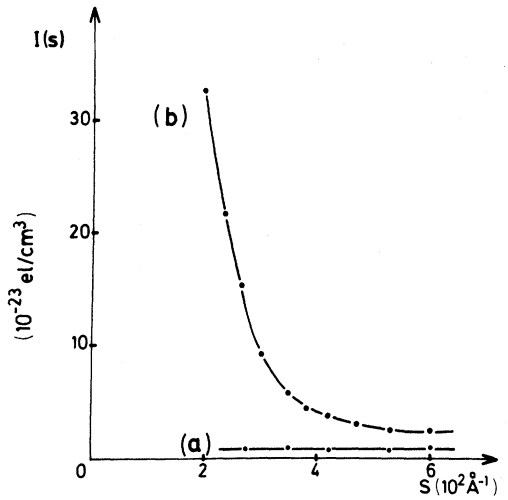

FIG. 1. Small-angle x-ray diffusion curve, $I(s)$, for mica implanted with oxygen (a) and iron (b) ions. (a) Only point defects are observed. (b) The sharp rise of $I(s)$ for small values of s indicate that extended defects are present. Their contribution superimposes on the flat background due to point defects observed for large values of s.

sent the electron-density deficits associated with both types of defects, while $n(R)$ and $N(R)$ refer to the linear density (number per micrometer of range) of the point defects and the extended defects, respectively.

The size of extended defects, which play a dominant role in our model, is a complex concept that we illustrate in Fig. 2. In this figure, we plotted two plausible distributions of $\Delta\epsilon$ within an extended defect as a function of the distance to the center. The analysis of the diffusion curve yields two constraints on these distributions; the existence of "wings" and a concave maximum. As the exact shape of the adequate distributions does not markedly affect the predictions of our model (see Sec. IV B), we selected a Gaussian distribution, and the size of the extended defects is then scaled by the halfwidth of this distribution.

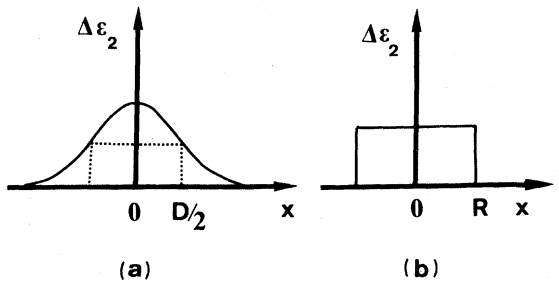

FIG. 2. Model profiles of the electronic-density deficit across an extended defect. (a) Gaussian. (b) square step.

The major limitation of the x-ray analysis is that only the product $N(R)\Delta\epsilon_2^2$ is directly measured. As $\Delta\epsilon_2$ cannot be determined from these studies, this method only yields the *relative* variations of the linear density of extended defects along the range.

C. Etched-tracks measurements

The etching conditions used to reveal the etchable tracks are summarized in Table II, where we report for mica, labradorite, and olivine the "standard etching time," t_0, required to produce fission-fragment tracks easily observable with an optical microscope.[12] Larger etching times used in our work, intended to reveal tracks with very small etching rates, will be expressed in units of t_0.

The optical microscope can only be used to measure the length of tracks with relatively high etching rates. In fact, with this instrument a track can only be identified as such when its depth-to-diameter ratio exceeds a critical value[12] (~0.25). However, we also investigated tracks with a very low etching rate, which corresponds to tracks partially annealed and/or registered in the vicinity of the so-called "registration threshold." For such low etching rates, the etching time has to be increased up to $>100t_0$, and the tracks then appear as shallow etch pits which can only be observed with a scanning electron microscope or an optical microscope with a Nomarsky phase contrast attachment.

In this paper we will refer to the tracks produced by a given ion as the $Z(X)$ tracks, where Z corresponds to the atomic symbol and X to the energy of the incident ion. The length distribution of the tracks first annealed at a temperature T for two hours, then etched during a time t starting from a total range R_0, will be quoted as the $D_L\{R_0; (t, T)\}$ distribution. In the case of labradorite, these distributions always exhibit a single peak. This allowed us to determine the bulk etch rate of the tracks, $V_b(R)$, as a function of the residual range R. In mica, such a determination was not possible, as the observation of double-peak structures prevented the measurement of a significant mean track length.

III. EXPERIMENTAL RESULTS

A. Latent-track studies

1. Mica and olivine before a thermal annealing

Below a critical atomic number (~10 for mica), the linear density of extended defects drops below the detection threshold of the x-ray apparatus, and

TABLE II. Etching conditions and "standard" etching time t_0.

Mineral	Reagent	Temperature	t_0
Muscovite mica[a]	HF 40%	25 °C	20 min
Labradorite[b]	6g NaOH, 8g H_2O	120 °C	40 min
Olivine[c]	10g EDTA, 25g H_2O 0.25 cc H_3PO_4, 0.25g $C_2O_4H_7$ adjusted to pH 8	120 °C	200 min

[a] P. B. Price and R. M. Walker, J. Appl. Phys. 33, 3407 (1962).
[b] D. Lal, A. B. Muralli, R. S. Rajan, A. S. Tamhane, J. C. Lorin, and P. Pellas, Earth Planet Sci. Lett. 5, 111 (1968).
[c] S. Krishnaswami, D. Lal, N. Prabhu, and A. S. Tamhane, Science 174, 287 (1971).

only point defects are observed along the range. Furthermore, for ions heavier than krypton, the size of the extended defects becomes larger than ~40 Å, and they are not detectable with the x-ray wavelength used (Cu $K\alpha$, $\Lambda \sim 1.54$ Å).

The size of extended defects can be considered as constant when the incident-ion energy varies from ~0.2 MeV/amu to 10 MeV/amu (Table III). For example, in this energy range the size of the extended defects generated by argon ions is constant within 10%. From argon to krypton, the size of extended defects increases by about a factor of two.

In mica, the relative variations of the linear density $n(R)$ of point defects fit closely those of the two functions widely used in previous work[13,18]: the total rate of energy loss, dE/dR, and the rate of primary ionization J. In striking contrast, the linear density $N(R)$ of extended defects decreases by a factor of seven from 1 MeV/amu to 7 MeV/amu, while J and dE/dR decrease by $\lesssim 50\%$ (Fig. 3). In olivine, the relative variation of $N(R)$ is similar, although extended defects now have a square-step profile (Table III).

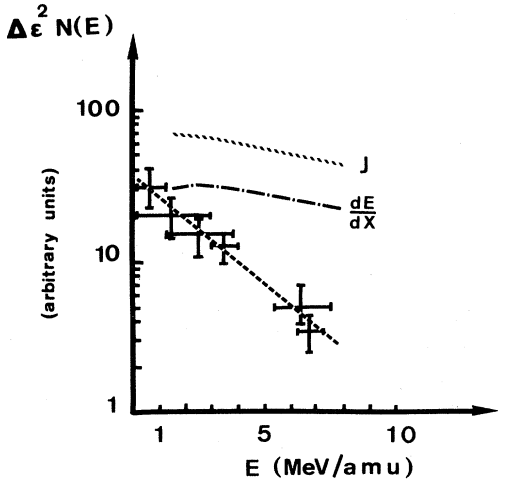

FIG. 3. Relative variation of the linear density $N(E)$ of extended defects derived from x-ray observations of mica irradiated by Fe ions. $N(E)$ drops much more rapidly when E increases than both the primary ionization rate J and the energy-loss rate dE/dx.

2. *Mica and olivine after a thermal annealing*

In mica, upon thermal annealing the point defects first disappear at a temperature $T_1 \sim 300$ °C, whereas a temperature $T_2 \sim 420$ °C is required to trigger a noticeable alteration of the extended defects. Then, the annealing of the extended defects occurs from T_2 up to a temperature $T_3 \sim 500$ °C, at which they are no longer observable within the limit of sensitivity of the x-ray apparatus (T_1, T_2, and T_3 refer to two hours annealing runs). In olivine, the same type of behavior is observed, although the temperatures T_2 and T_3 are now ~50 °C smaller. In a given mineral, T_1 is independent on both Z and E, and the annealing of point defects can be characterized by an Arrhenius-type equation corresponding to an activation energy of ~0.8 eV.[17]

The annealing of extended defects in mica present two unexpected features:

(i) For $T > T_2$, a complex change in the structure of the extended defects is observed. The distribution of the electronic-density deficit reported in Fig. 2 loses its wings, switching to a "square-step" distribution. Then, the width of this partially annealed defect remains constant up to T_3, while the maximum electronic-density deficit slowly decreases until the difference in contrast between the defect and the host material is no longer detectable.

(ii) $N(R)$ is not changed as long as the annealing temperature does not exceed T_3.

B. Etched-track studies

We present a selection of results on etched external tracks which could not be interpreted be-

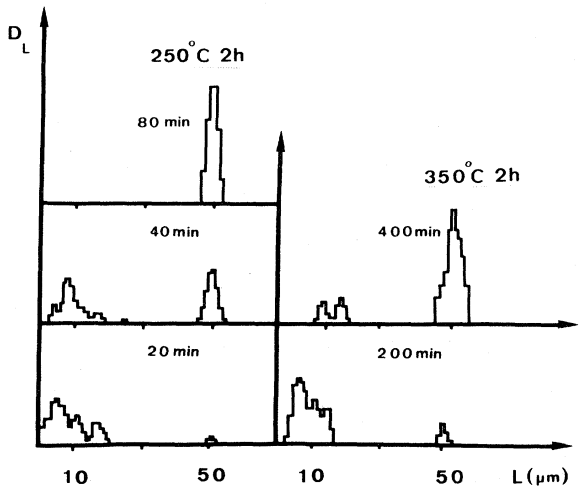

FIG. 4. Length distribution of tracks produced in mica by 7-MeV/amu Fe ions as a function of the etching time t, after low-temperature annealings.

fore and which represent severe constraints on any model dealing with the registration of tracks in dielectric minerals. We investigated the length distributions of tracks in mica, labradorite, and olivine, as well as the bulk etching rate, $V_b(Z, R)$, of tracks in labradorite. Furthermore we measured in the same minerals the variation of the track density as a function of the annealing temperature.

1. *Fe and Kr tracks in muscovite mica*

Before annealing, for both Fe(7) and Kr(6) tracks, the track-length distribution $D_L\{R_0; (t_0, T)\}$ present a narrow maximum centered at the total range R_0 [~51 μm for Fe(7) and ~43 μm for Kr(6)]. The position and width of this peak do not vary when the etching time is increased. When the energy of the incident ion decreases, these distributions keep the same width while the peak position still corresponds to the total range of the ion R_0.

TABLE III. Size of extended defects in mica and olivine.

Mineral	Ion	Size
Muscovite mica[a]	Ne	15 Å
	Ar (1 MeV/amu)	22 Å
	Ar (10 MeV/amu)	20 Å
	Fe	26 Å
	Kr	>26 Å
Olivine[b]	Ar	32 Å
	Fe	38 Å
	Kr	>40 Å

[a] Assuming a Gaussian profile.
[b] Assuming a square-step profile.

A thermal annealing triggers the following changes in the $D_L\{R_0;(t, T)\}$ distributions:

(i) After a low-temperature annealing ($T < 400$ °C), the Fe(4) and Kr(6) distributions are not modified. However, the length distribution of Fe(7) tracks now exhibits a double-peak structure (Fig. 4). A fraction of the tracks are still etched up to the total range R_0, the others having much smaller lengths (~10 μm). The main effect of an increase in the etching time is to deplete the 10-μm peak to the benefit of the total range peak. Finally, the partially annealed length distribution switches back to the unannealed one when the standard etching time t_0 is multiplied by a factor $\alpha(T)$, where $\alpha(T)$ is a scaling factor which completely describes the effect of a low-temperature annealing. We have for any etching time t

$$D_L\{R_0;(\alpha(T)t, T)\} = D_L\{R_0;(t, 20\,°\mathrm{C})\}.$$

$\alpha(T)$ is about 4 and 30 when the annealing temperature is 250 and 350 °C, respectively.

(ii) In the high-temperature range ($T > 400$ °C), the Fe(7) tracks cannot be observed even after very long etching times ($>100t_0$). In addition, the Fe(4) and Kr(6) length distributions present a double-peak structure which persists when the etching time is increased.

The length distribution of tracks in mica cannot be used to define a mean etching rate, $V_b(R)$, as this requires the determination of the average track length as a function of time, which is meaningless for double-peaked distributions. A very specific additional observation can be made in mica, which considerably helped us in developing the track-etching model presented in Sec. IV. When observed with the SEM (scanning electron microscope) or the Nomarsky phase-contrast optical microscope, the superficial etch pits of partially annealed tracks present a very spectacular terrace structure (Fig. 5). Such terraces can be characterized both by their lateral width and their linear density along the track, which critically depend on the residual range of the incident ion and the annealing temperature.

2. *Fe and Kr tracks in labradorite*

Track-length distributions in labradorite show a single-peak structure[8] (Fig. 6) which directly yields the variations of the track-etching rate, $V_b(R, T)$. Before thermal annealing, the $V_b(R, 20\,°\mathrm{C})$ curves measured for Fe and Kr exhibit two distinct behaviors (Fig. 7): The Fe curve presents a broad maximum located at $R \sim 8$ μm and limited by two steeply falling edges, as well as a slowly decreasing tail for large values of R (>20

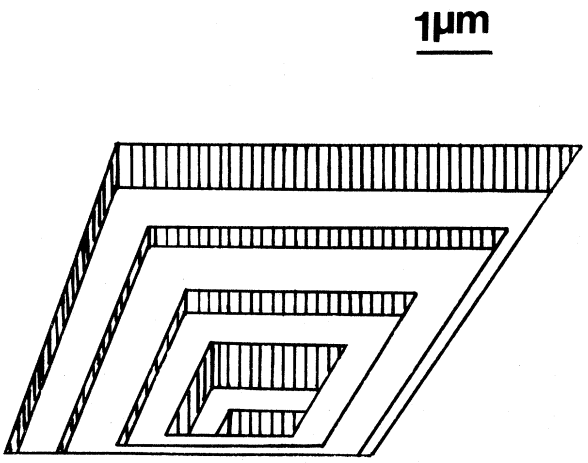

FIG. 5. Typical terrace structure of Fe (7) tracks in mica after an annealing at 350 °C (2 h) and 200 min of etching.

μm). In contrast, the Kr curve exhibits a large plateau extending over a range interval of ~30 μm.

The variations of $V_b(R,T)$ with the annealing temperature indicate the existence of two distinct annealing steps:

(i) The low-temperature annealing ($T<400$ °C) does not alter the shape of the $V_b(R)$ curve relevant to Kr tracks. However, the etching speed $V_b(R)$ of Fe tracks decreases by an approximately constant factor (~1.4 at 300 °C), while both the position and width of the peak is not changed.

(ii) After a high-temperature annealing ($T>400$ °C), the peak in the Fe curve shrinks in both extension and height (Fig. 7) around its maximum at ~8 μm. At 600 °C, the maximum value of $V_b(R)$ drops to about $2V_0$, where V_0 refers to the etching rate of the unirradiated mineral along the track direction. The $V_b(R)$ curve for Kr tracks starts to be noticeably altered at much higher temperatures. For instance, at $T\sim700$ °C (2 h), the extension and height of the plateau have decreased down to ~20 μm and $5V_0$, respectively.

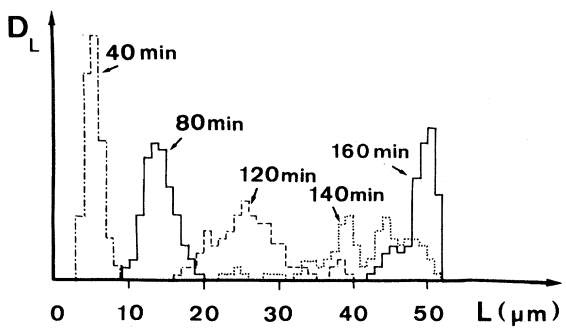

FIG. 6. Length distribution of unannealed Fe (7) tracks in labradorite as a function of the etching time t.

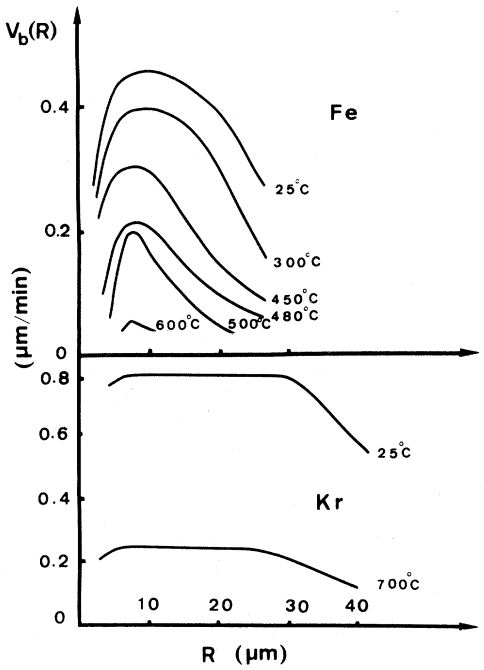

FIG. 7. Etch rate $V_b(R,T)$ of Fe and Kr tracks in labradorite as a function of the annealing temperature.

3. *Fe tracks in olivine*

We have not obtained in this mineral sufficient data to plot the $V_b(R)$ curves. Indeed, there are two specific difficulties attached to this determination:

(i) Etching times up to $100t_0$ are required to derive $V_b(R)$. In olivine, this is impractical due to the very high value of t_0 (~300 min).[12]

(ii) In this mineral, the hollow canals that delineate the etched tracks are highly asymmetric and the length of short tracks cannot be measured with a good accuracy.

However, the following preliminary observations show that the registration of Fe tracks in olivine follows the general rules established for mica and labradorite: (i) Before thermal annealing, the track-length distribution shows a single-peak corresponding to the total range of the ions, as in mica. (ii) After a low-temperature annealing ($T<350$ °C), the track-length distribution switches back to the unannealed one when an etching time $t=\alpha(T)t_0$ is used [$\alpha(T)\sim1.6$ at 300 °C]. (iii) Fe (4) tracks are no longer observable with the optical microscope when $T>400$ °C.

4. *Variations of the track density with the annealing temperature*

For all the minerals and ions so far investigated,

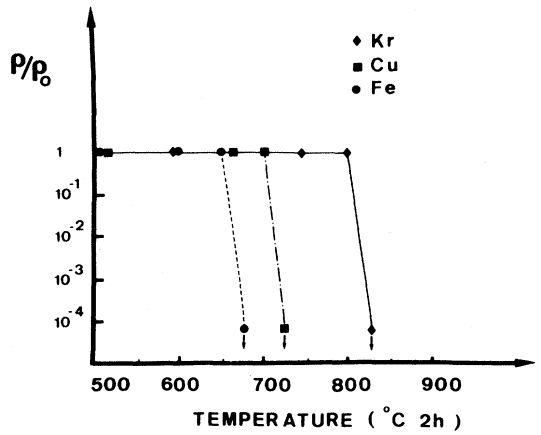

FIG. 8. Etching efficiency $\rho(T)/\rho_0$ of tracks produced in labradorite by Fe, Cu, and Kr ions with an energy of 1 MeV/amu.

the track density $\rho(T)$ drops sharply over a narrow temperature range (~50 °C) around a critical temperature T_c.[8] The value of T_c is defined by requiring that

$$\frac{\rho(T_c)}{\rho_0} \lesssim 10^{-4},$$

where ρ_0 corresponds to the unannealed value of the track density. T_c varies with both the characteristics of the incident ions and the nature of the mineral, but it also depends on the observational technique. For example, the value of T_c for Fe tracks observed in mica with an optical microscope is ~50 °C smaller than that derived with the SEM. To establish a reliable scale of T_c values, we used only SEM observations. In Fig. 8 we present a selection of our results concerning tracks of monokinetic ions in labradorite ($E \sim 1$ MeV/amu). T_c varies from ~670 °C for Fe (1) tracks to ~730 °C and ~830 °C for Cu (1) and Kr (1) tracks, respectively.

IV. THE GAP MODEL FOR THE REGISTRATION OF ETCHABLE TRACKS IN DIELECTRIC MINERALS

Previous models, as reviewed recently by Fleischer,[19] were based on the concept of a threshold mechanism for the formation of etchable tracks. In such models, a continuous trail of radiation damage (the latent track) can only be formed within a narrow-range interval $\Delta R(Z)$, near the end of the range of the incident ion where the rate of primary ionization J, or the rate of "restricted" energy loss[18] exceeds a critical value. This critical value would depend on the nature of the mineral, being much larger in olivine than in mica. As the latent tract is much more chemically reactive than the host material, an etchable track would thus be formed in the same range. Such models could account neither for the detailed shape of the track-length distributions, nor the annealing behavior of the tracks. All external tracks formed by a given ion at a given energy should have the same length, in contradiction with the observation of a double-peak structure for partially annealed Fe (7) tracks in mica. Therefore, any improved model dealing with track registration should issue detailed predictions on the complex shape of track-length distributions. In addition to these critical observations, it should also account for the terrace structure of partially annealed tracks in mica (Fig. 5), the distinct effect of a low- and a high-temperature annealing, and the very sharp drop of the track density around a critical temperature T_c.

A. The model

Our model, which has been briefly presented previously,[8] is derived from the existence of two populations of defects in the latent tracks and the observation that extended defects play the dominating role in the etching of the tracks because their annealing, but not that of the point defects, triggers irreversible changes in track-length distributions. In our model we thus consider that each extended defect induces the formation of a "core zone" along the track. Such core zones can be characterized with an effective length λ_c, in which the etching rate V_c is far greater than that of the unirradiated crystal V_0, in the track direction. Therefore, we assimilate the variation of the etching rate across this zone to a square-step function. As a consequence of low values of the linear density $N(R)$ of extended defects and/or statistical fluctuations, the distance between the centers of two consecutive extended defects can be greater than λ_c. In this case, a "gap zone" with a length d appears between the two core zones, which contains only point defects. These gap zones are etched out at a rate V_g much lower than V_c, but still higher than V_0 due to the presence of point defects. As the x-ray measurements show that the density $n(R)$ of point defects does not vary markedly along the range, we considered V_g as constant as a first approximation.

For a given ion, the probability p that the distance between two successive extended defects exceeds λ_c is

$$p = \exp[-N(R)\lambda_c].$$

Along one micrometer of range, $N(R)$ such intervals are encountered and the linear density $N_g(R)$ of gap zones is thus

$$N_g(R) = N(R)\exp[-N(R)\lambda_c].$$

In addition, the mean aggregated length $w(R)$ of gap zones per micrometer of range is

$$w(R)=\exp[-N(R)\lambda_c]$$

and the mean length $\bar{d}$ of gap zone is

$$\bar{d}=\frac{1}{N(R)}.$$

The etching time needed to etch out a 1-μm-long track segment represents the sum of the etching times required to etch out all the constituent gap zones and core zones. The mean etching rate $V_b(R)$ is thus given by

$$V_b(R)=\frac{1}{\frac{w(R)}{V_g}+\frac{[1-w(R)]}{V_c}}$$

$$=\frac{V_c}{1+(V_c/V_g-1)\exp[-N(R)\lambda_c]}.$$

We finally obtain the average length $L(R_0,t)$ of a track etched for a time t, and that intersects the observation plane at a residual range R_0:

$$t=\int_{R_0-L}^{R_0}\frac{dR}{V_b(R)}.$$

These mean values of the etching rate and etched length can be directly compared with the corresponding experimental values, but they cannot yield the detailed track-length distribution. Consequently, we developed a Monte Carlo code that generates large numbers of theoretical tracks. In these computations, a given latent track is divided into successive segments one micrometer long, located at a residual range R_t. Extended defects are randomly distributed over each one of the track segments in agreement with the value of the local density $N(R_t)$. From this distribution we derive $w(R_t)$, the aggregated length of gap zones, and the etching time $\delta_t t$, required to etch out each track segment:

$$\delta_t t=\frac{w(R_t)}{V_g}+\frac{[1-w(R_t)]}{V_c}.$$

Starting from the total range R_0, we proceed from one segment to the next, until the available etching time is expended:

$$\sum_1^n \delta_t t>t.$$

The etched length along this specific theoretical track is then

$$L_0=R_0-R_n.$$

It must be noted that the observation plane is simultaneously etched, and the "observable" etched length is thus

$$L=L_0-\frac{V_p}{\sin\theta}t,$$

where V_p is the etching rate of the plane, and θ the angle between the track and the plane. In this way, the code generates a large number of observable track lengths which can be compared to the observed track-length distribution. In this model the differences observed between the tracks produced by a parallel beam of monokinetic ions are easily interpreted in terms of statistical fluctuations in the distribution of extended defects from one track to the next.

There are several predictions of this model that do not depend on the actual values of its parameters and which will be discussed in the following section. However, the computation of track-length distributions does require the determination of five basic parameters, namely the linear density of extended defects, $N(R)$, the effective length of core zones, λ_c, and the three etching rates, V_0 V_g, and V_c.

B. Determination of the five basic parameters of the model

We present below a determination of the five basic parameters of the model which does not involve any fitting between the theoretical and experimental distributions. However, these determinations are still in part, model dependent, as they rely on the existence of gap zones along the latent track.

Value of V_0, etching rate of the unirradiated mineral along the track direction. For a given set of etching conditions, the value of V_0 will result from the contribution of the V_{hkl} rates which refer to etching rates evaluated perpendicularly to the various crystallographic planes. Our method to determine the set of V_{hkl} rates, which will be reported in detail in a forthcoming paper, can be outlined as follows. Let us consider a tiny spherical hole reached by the reagent within the crystal. Upon etching, a polyhedral cavity (the etch polyhedron) limited by crystallographic planes corresponding to the smallest V_{hkl} values will be formed. For tracks due to heavily damaging ions, such as fission fragments, the etching rate along the latent tracks, $V_b(R)$, far exceeds any one of the V_{hkl} rates. For appropriate etching conditions, the etched track then looks as a hollow-etch canal with a constant section which delineates the envelope of the etch polyhedrons formed almost simultaneously along the etchable range of the incident ion. The intersection of this etch canal with the observation plane gives a superficial etch pit which reflects the projection of the etch polyhedron on the observa-

tion plane along the direction of the track. Through an analysis of the various etch pits observed on a given plane, it is thus possible to derive the etch polyhedron. In this context, mica and labradorite represent two extreme examples of etching behavior. In mica, the observation plane is always the perfect cleavage plane (001), and the corresponding etching rate V_{001} (~2 Å/min) is about 100 times smaller than the two etching rates V_{100} and V_{010} (~250 Å/min) for the etching conditions defined in Sec. II. Consequently, in this highly anisotropic case, the V_0 value will be adequately approximated by

$$V_0 = \frac{V_{001}}{\sin\theta},$$

where θ is the angle between the track and the observation plane. In contrast, in labradorite the etching rates V_{hkl} (300 Å/min to 600 Å/min) are much less anisotropic. In this case, the V_0 value can be assimilated to the mean value of ~400 Å/min as a first approximation. Olivine corresponds to an etching behavior intermediate between those of mica and labradorite, as the slowest etching rates differ by a factor of ~5 in this mineral.

Value of V_g, etching rate in gap zones. V_g is the only parameter that depends on the density of point defects. As the x-ray measurements clearly show that the point defects, but not the extended defects, are affected in the low-temperature range ($T < 400$°C), V_g will be the only parameter to vary upon a low-temperature annealing. From the gap model, the track-length distributions should then exhibit a scaling behavior ruled by the total length of the gaps etched, $V_g(T)t$. Indeed, distributions measured after a low-temperature annealing match the unannealed distribution when the etching time t is multiplied by a constant factor $\alpha(T)$, which depends on the mineral (see Sec. III). We can thus conclude that

$$V_g(T) = V_0 \frac{\alpha(T_1)}{\alpha(T)},$$

where T_1 is the temperature at which all the point defects have been annealed. When the annealing temperature is larger than T_1, the etching rate in gap zones is simply that of the unirradiated mineral V_0.

Value of V_c, etching rate in core zones. The determination of this etching rate is only required to compute length distributions corresponding to tracks heavily loaded with extended defects. In this case, the integrated etching time of the core zones is not negligible with respect to that of the few residual gap zones. From the gap model, we predict a saturation in the value of $V_b(R)$ as soon as the core zones start to overlap near the maximum of the linear density $N(R)$ of the extended defects. This is in good agreement with the experimental measurements of $V_b(R)$ in labradorite, which exhibits a plateau value for Kr ions and a broad maximum for Fe ions near the maximum of $N(R)$. We thus assimilate V_c to such saturation values of $V_b(R)$. In mica, these saturation values are at least 10^4 times larger than V_0 and can be considered infinite.

Value of $N(R)$, linear density of extended defects. As already stated in Sec. II, x-ray measurements only yield the relative variations of $N(R)$ along the range of a given ion. We have thus to determine the absolute value of this parameter at a given range to completely define the $N(R)$ curve. This is possible in mica due to the very specific terrace structure of etched tracks in this mineral. In our model, such terraces reflect the occurrence of a gap along the latent track for a mineral in which V_c is much higher than V_g and V_0. Indeed, a single gap can then delay the etching of the track for a significant amount of time, while the diameter of the overlaying etch canal continuously widens at the rate V_{100}. When the reagent has etched out the gap at the relatively low rate V_g, the difference δ between the diameters of the etch canal above and below a given gap will be

$$\delta = 2d \frac{V_{100}}{V_g},$$

where d is the width of the gap. From the measurement of δ for many gaps at a given residual range R, we can thus infer the mean value $\bar{d}$ of d, which in turn yields the absolute value of $N(R)$ as

$$N(R) = 1/\bar{d}.$$

Relying on this model-dependent method, we obtained for mica the values of $N(R)$ reported on Fig. 9 for Fe and Kr tracks. In order to derive $N(R)$ for other silicates, we assumed as a first approximation that the $N(R)$ distribution is the same for all silicates. This critical assumption is compatible with both the similar relative variations of $N(Z,R)$ in mica and olivine and the predictions of the track-formation mechanism qualitatively outlined in Sec. V C. In addition, the validity of this assumption is severely tested when one is trying to compute track-length distribution in labradorite. Indeed, in this mineral only the absolute values of $N(Z,R)$ determined for mica do reproduce the striking features of the corresponding experimental distributions.

Value of λ_c, effective length of the core zones. The variations of λ_c with the characteristics of the incident ions, the annealing temperature, and the nature of the mineral, originate from the corresponding variations in the size and the shape of the

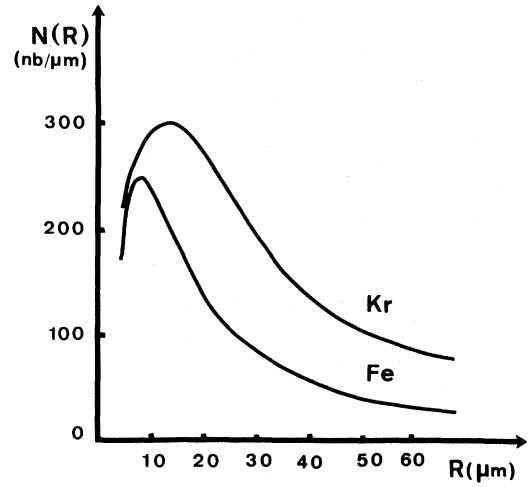

FIG. 9. Linear density $N(R)$ of extended defects produced by Fe and Kr ions in mica.

extended defects. Consequently, we assumed that the relative variations of λ_c closely match the structural changes of the extended defects inferred from x-ray measurements. In particular, as extended defects are not affected by a low-temperature annealing, λ_c is constant within this temperature range. We determine the absolute value of λ_c in two different ways:

(i) In minerals such as labradorite, where the V_{hkl} etching rates are relatively isotropic, gap zones cannot completely block etching. Consequently, the bulk etching rate $V_b(R)$ varies smoothly with R and can be determined with a good accuracy. We select a region in which $V_b(R)$ is much lower than V_c, thus heavily loaded with gap zones. In this case

$$V_b(R) = V_g \exp[N(R)\lambda_c] .$$

λ_c can thus be inferred from a single measure of $V_b(R)$.

(ii) In mica, a single gap can block etching for partially annealed tracks, forming a terrace. We can determine λ_c by measuring the linear density of gaps, $N_g(R)$, at a given residual range, as

$$N_g(R) = N(R) \exp[-N(R)\lambda_c] .$$

It must be noted that the values of λ_c determined by these two methods (Table IV) are much larger than the sizes of the extended defects (Table III). Thus, even the weak wings of the Gaussian-shaped extended defects seem to enhance the etching rate by a large factor.

V. DISCUSSION

A. Comparison of the model with experimental results

As discussed above (Sec. IV B), two main observations are already predicted by the gap model without considering the values of the five basic parameters: (i) Upon low-temperature annealing, only V_g is changed. Thus, the track-length distribution after an etching time t should match the unannealed distribution corresponding to the etching time $tV_g(T)/V_g(20\,^\circ\mathrm{C})$, in good agreement with our observations. (ii) The terrace structure of partially annealed tracks observed in muscovite mica is a direct consequence of the gap model in a mineral where the etch rates V_{hkl} are highly anisotropic.

We computed track-length distributions in mica and labradorite as well as the mean etching rate of Fe tracks in labradorite, both before and after a thermal annealing, using the values of the five basic parameters determined in Sec. IV B. We show that the critical observations reported in Sec. III are well reproduced by these computations. This strongly supports the validity of the gap model.

1. Mica

Before annealing, the length distribution of Fe (7) tracks etched 20 min, which exhibits a single peak at $L = R_0$, can be reproduced using our derived λ_c value of ~700 Å and a V_g rate of ~360 Å/min [Fig. 10(c)]. The total gap length etched is

TABLE IV. Effective length λ_c in labradorite, mica, and olivine.

Mineral	Ion (annealing temperature)	Effective length
Labradorite	Fe (25 °C)	~270 Å
	Fe (500 °C)	~120 Å
	Kr (25 °C)	~350 Å
	Kr (700 °C)	~200 Å
Muscovite mica	Fe (25 °C)	~700 Å
	Fe (450 °C)	~430 Å
	Kr (25 °C)	~900 Å
Olivine	Fe (25 °C)	~60 Å

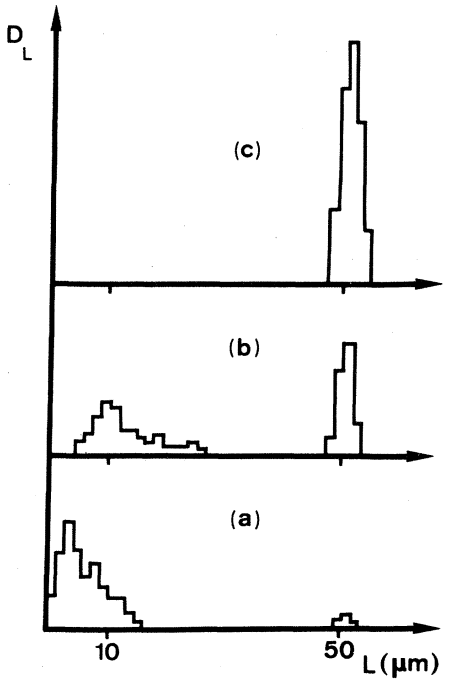

FIG. 10. Length distributions of Fe (7) tracks in mica, computed from the gap model. (a) $V_g(T)t = 1800$ Å, (b) $V_g(T)t = 3600$ Å, (c) $V_g(T)t = 7200$ Å.

then ~7200 Å, whereas that of the gaps present in the high-energy part of the range [N_g(50 μm) ~2.5/μm] is only ~4000 Å (Fig. 11).

A low-temperature annealing ($T < 400$ °C) results in lower values of V_g. From the etching time required to etch all the tracks up to the total range, we derived values of V_g of 90 Å/min and 12 Å/min for annealing temperatures of 250 and 350 °C, respectively. In this temperature range, λ_c remains constant. For etching times such as 20 min (250 °C annealing) corresponding to low values of the total gap length etched (~1800 Å), the gaps in the high-energy part of the range (25 μm to 50 μm) block the etching, and all the tracks are short [<20 μm; Fig. 10(a)]. When the etching time is doubled, the total gap length etched also doubles (~3600 Å). In favorable tracks, the reagent breaks through the last gap and rushes through the region 25–2 μm, where no gaps are present (Fig. 11). Then, a population of tracks with lengths close to the total range is observed [Fig. 10(b)]. When the total gap length etched reaches ~7200 Å (t ~80 min), all tracks are etched up to the end of the range, thus matching the unannealed distribution. This very good fit with the complex behavior of Fe track-length distributions in mica (Fig. 4) strongly supports the discontinuous etching process we propose.

After a high-temperature annealing ($T > 400$ °C), only tracks almost devoid of gaps can still be etched due to the very low value of V_0 (~2 Å/min). Thus, Fe (4) tracks (R_0 ~28 μm) but not Fe (7) tracks (R_0 ~51 μm), can still be etched. Kr tracks have higher linear densities of extended defects (Fig. 9) with a greater effective length λ_c (Table III). Thus, they can still be etched at a greater residual range [R_0 ~43 μm for Kr (6) tracks] and are more thermally stable than Fe (4) tracks.

2. *Labradorite*

In this mineral, the absolute value of V_0 is much larger (~400 Å/min). This implies that after 20 min of etching, hundreds of gaps will have been etched. Therefore, the statistical variations from one track to the next are smaller than in mica, and the track-length distributions exhibit a single-peak structure. Theoretical distributions corresponding to λ_c ~270 Å (Table IV) and V_0 ~400 Å/min (Fig. 12), well reproduce the experimental ones (Fig. 6). For this mineral, $V_b(R)$ can also be derived directly from the model. In the low-temperature range, λ_c is constant and V_g decreases by a factor ~1.4. In the high-temperature range, V_g is now constant and λ_c starts to decrease. Following these guidelines, we are able to well match the observed mean etching rates for Fe tracks (Fig. 13). The observed plateau in $V_b(R)$ curves corresponding to krypton is easily interpreted, as the high values of $N(R)$ and λ_c induce a complete overlapping of the core zones, $V_b(R) \sim V_c$.

3. *Variation of the track density ρ with the annealing temperature*

The ratio $\rho(T)/\rho_0$ is usually defined at the "etching efficiency" η, of tracks after a given annealing. As shown previously,[12] it is directly linked with the ratio $V_b(R)/V_0$, which was not related to the structure of the latent tracks. In our model we have now

$$V_b(R)/V_0 = \exp[N(R)\lambda_c] .$$

This ratio is thus very sensitive to small changes in λ_c, and a small increase in the annealing temperature can induce an abrupt drop in the etching efficiency. Such a behavior could not be interpreted with models assimilating the track to a single "defect" annealing in accordance with an Arrhenius equation.

We emphasize that we have been able to interpret two etching behaviors as different as those of muscovite mica and labradorite only by assuming *the same distribution* $N(R)$ of extended defects along the ion range. This supports our assumption that differences between silicates arise mainly not from *track registration*, which leads to the $n(R)$

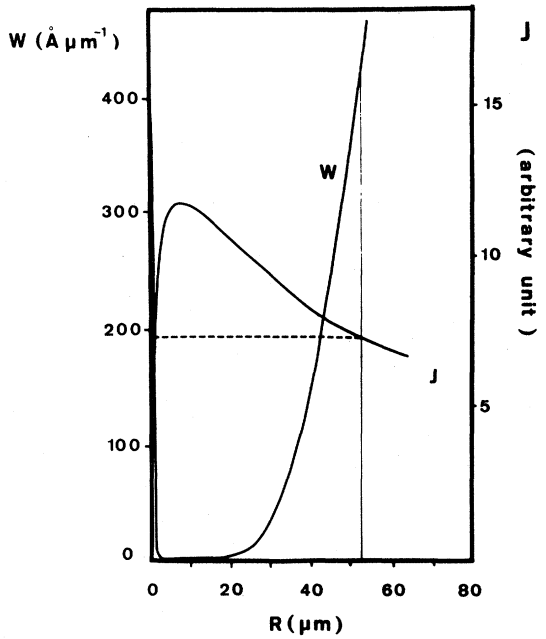

FIG. 11. Aggregated gap length per micrometer, $w(R)$, for unannealed Fe tracks in mica ($\lambda_c = 700$ Å). For comparison, the primary ionization rate is shown together with the "threshold" corresponding to an etchable range of 52 μm.

and $N(R)$ distributions of defects, but from *track revelation*, well described by the V_g and λ_c parameters.

B. Discussion of previous concepts on etched-track registration

Most applications of fossil-track studies in natural minerals originate from the registration of internal latent tracks within the volume of a mineral grain. These tracks can be produced by a variety of track-forming events such as spontaneous fission and slowing down cosmic-ray nuclei, and their spatial distribution is generally isotropic. The latent tracks can be "externally etched" on a polished surface, or "internally etched" using cleavages to conduct the reagent inside internal tracks that intersect such surfaces.[20]

These studies relied on a threshold mechanism for the formation of etchable tracks: Only parts of the range in which the ionization rate (or the restricted energy loss) exceeded a critical value, specific to the mineral, could be revealed through etching, thus defining an etchable range, $\Delta R(Z)$. This parameter $\Delta R(Z)$ allowed us to convert track-length distributions into elemental abundances, and to link the track density observed on a plane, ρ, to the volume density of track-forming events, ν. It

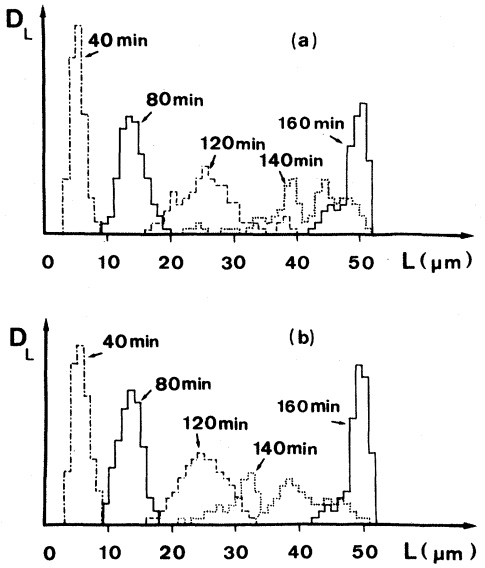

FIG. 12. Experimental (a) and theoretical (b) distributions of unannealed Fe (7) tracks in labradorite as a function of the etching time t. The theoretical distributions were derived for $\lambda_c = 270$ Å and $V_g = 560$ Å/min.

is directly related to the etching efficiency, $\eta(R)$, the proportion of tracks crossing the observation plane at a residual range R which are revealed through etching. However, it has been shown that such a track-forming process is not consistent with several experimental results: (i) Extended defects are still observed when the ion range cannot be revealed through etching. (ii) Track etch rates vary continuously along the range down to the etch rate of the unirradiated mineral.

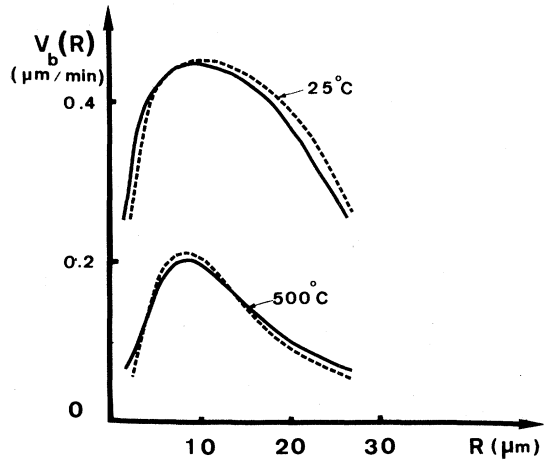

FIG. 13. Experimental (dashed line) and theoretical (solid line) etch rates $V_b(R,T)$ for Fe tracks in labradorite, before and after a high-temperature annealing at 500 °C (2 h). The theoretical curves correspond to $\lambda_c = 270$ Å, $V_g = 560$ Å (unannealed), and $\lambda_c = 150$ Å, $V_g = 400$ Å (annealed at 500 °C).

In our model, this apparent threshold can be interpreted from the very abrupt increase of the proportion of gaps in two specific parts of the range: For Fe tracks in mica, this proportion increases from 10^{-3} to 1 over the last two micrometers of the range. It also doubles between 40 and 50 μm of residual range, whereas the ionization rate drops by only 10% (Fig. 11).

To clarify the concepts of etchable range and etching efficiency, let us consider an isotropic distribution of internal tracks with a volume density ν, of track-forming events in an isotropically etching mineral. The etching efficiency on a polished section can be derived as follows. Tracks intersecting the plane at a residual range R etch faster than the plane itself only if

$$V_b(R)\sin\theta > V_p ,$$

where θ is the angle between the track and the plane, and V_p is the etching rate of the plane. Furthermore, the revealed track can only be recognized as such if its depth-to-diameter ratio exceeds a minimum value β, characteristic of the observational method (β is larger for an optical microscope than for a scanning electron microscope or a Nomarsky phase-contrast optical microscope). This depth-to-diameter ratio can be readily derived from the bulk etch rate $V_b(R)$ of the track. The observability condition becomes

$$\sin\theta > \frac{V_p}{V_b(R)}\left\{1+2\beta\left[\left(\frac{V_b(R)}{V_p}\right)^2-1\right]^{1/2}\right\}^{1/2} = \sin\theta_c .$$

The etching efficiency $\eta(R)$ is simply the proportion of tracks crossing the plane at the residual range R with an angle θ larger than θ_c:

$$\eta(R) = 1-\left(\frac{V_p}{V_b(R)}\right)^2\left\{1+2\beta\left[\left(\frac{V_b(R)}{V_p}\right)^2-1\right]^{1/2}\right\}. \quad (1)$$

The etching efficiency of fresh iron tracks in labradorite has been reported in Fig. 14. ~5% of the tracks cannot be observed even at the maximum of $V_b(R)$, while 5% of them can still be observed at ranges up to ~100 μm with an optical microscope. This demonstrates the inadequacy of a threshold etchable range outside which $\eta(R)$ would be 0.

For the same irradiation geometry the number of tracks intersecting the plane between the residual ranges R and $R+dR/2$, where ν is the volume density of track-forming events. Thus, the observed track density is simply

$$\rho = \frac{\nu}{2}\int_0^\infty \eta(R)dR .$$

If we set

$$\Delta R(Z) = \int_0^\infty \eta(R)dR ,$$

we obtain the classical formula

$$\rho = \frac{\nu\Delta R(Z)}{2} ,$$

extensively used in fission-track dating. However, there is a marked difference between our definition of the etchable range and the classical one. Indeed, the latter is independent on both the track-orientation and the observation technique. In contrast, the etchable range represents in our model a mean for all possible orientations. Furthermore, the etching efficiency $\eta(R)$ [Eq. (1)] and thus the etchable range depend on the observation technique. For a given track population, the observed track density will be larger with the SEM than with the optical microscope, due to the smaller value of β. This explains the apparent discrepancy between track densities measured in lunar material with these two instruments,[21] as well as much earlier observations.[6]

In a relatively isotropic mineral for a given observational method, Eq. (1) shows that $\eta(R)$ and $\Delta R(Z)$ depend only on the ratio $V_b(R)/V_p$. In our model, for regions loaded with gap zones we have

$$\frac{V_b(R)}{V_p} \sim \frac{V_g}{V_p}\exp[N(R)\lambda_0] .$$

In such minerals, the ratio V_g/V_p is small (<1.6 in labradorite and olivine). As we assume that the distribution $N(R)$ is similar in all silicates, the etchable range $\Delta R(Z)$ depends mainly on the effective length λ_c. λ_c can thus be considered as representative of the "sensitivity" of the mineral for track registration. For instance, $\lambda_c \sim 60$ Å and 270 Å for Fe tracks in olivine and labradorite, respectively, in agreement with the classical sensitivity scale.[12] In muscovite mica, for unannealed tracks, V_g is much larger than V_p. In addition,

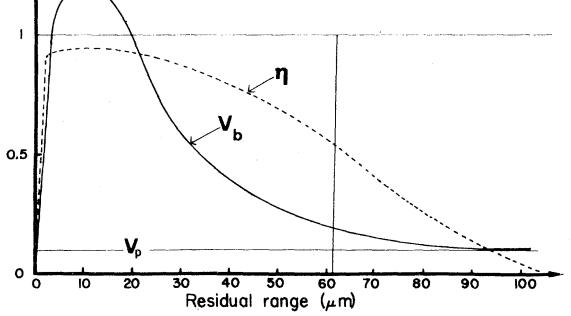

FIG. 14. Etching efficiency $\eta(R)$ of unannealed Fe tracks in labradorite as derived from the model (dashed line); variation of $V_b(R)$ as a function of range (solid line).

spurious etch pits do not develop on the surface. These two factors enhance track discrimination and, together with the large value of λ_c (~700 Å for Fe ions), explain why mica is among the most sensitive of all silicates. Upon a low-temperature annealing ($T \lesssim 400$ °C), the ratio V_g/V_p does not change markedly in olivine and labradorite, which thus keep their initial sensitivities. In contrast, this ratio decreases by a factor ~100 in muscovite mica, and the etchable range of Fe ions shrinks to ~30 μm, intermediate between olivine and labradorite, after a low-temperature annealing.

Let us now apply these new concepts to illustrate the limitations of previous track studies intended to infer the chemical abundance of very heavy cosmic-ray nuclei. For this purpose the external etching of a polished surface as well as methods in which the etchant reaches internal tracks registered within the mineral, were used. Such internal-etching techniques include the track-in-cleavage (TINCLE) method[20] (internal tracks intersecting cleavages can be reached by the etchant) and the track-in-track (TINT) method[22] (the etchant propagates along natural or artificial tracks reaching the external surface to the internal tracks they intersect). These internal-etching techniques were widely used because they were thought to yield the "full" etchable range of the tracks, which ought to be much less complex to interpret in terms of the atomic number of the incident ions than the partial length of tracks randomly cut by the external surface.

These three techniques all have the following major limitations: First, internal tracks intersect the cleavage, track, or external surface anywhere along the etchable range of the incident ion and this increases the spread of the track-length distribution.[10] Second, we have so far discussed the ideal case of a perfectly isotropic mineral. Even with the most appropriate etchant, slight anisotropies usually remain (e.g., within a factor of ~2 for labradorite in NaOH). Thus, internal tracks with favorable directions have longer etched lengths than tracks in perpendicular directions. Third, the natural annealing of fossil tracks further broadens track-length distributions.[9] Therefore, even the track-length distribution produced by a beam of monoatomic ions exhibits a quite large intrinsic spread.[9] In addition, there is a last severe limitation specifically attached to the TINT method. The external tracks that inject the etchant inside the internal tracks, enlarge upon etching by intersecting continuously new internal tracks. Thus internal tracks start to be etched anytime between 0 and the total etching time t_0. This peculiar effect, as illustrated in Fig. 6, further increase the spread of the track-length distribution.

Previous methods can only yield very broad abundance groups in cosmic rays with a mass resolution much worse than those previously claimed. Fortunately, a marked improvement in mass resolution can be achieved by relying on a new method originating from the gap model. This method already described[8] relies on track-density measurements performed after annealing at carefully selected temperatures. For example, in lunar labradorites, an annealing at 650 °C for 2 h completely erases tracks produced by iron-group ions, whereas tracks produced by ultraheavy ions can still be revealed. With such methods, a charge resolution of 5 to 10 may be expected for ultraheavy ($Z > 30$) and superheavy ions.

C. Present limitations of the gap model

The radiation damage mechanism responsible for the formation of both point defects and extended defects is not yet understood and we cannot predict the values of $N(R)$ for a given ion. Consequently, when extending the model to other targets, we rely on the assumption that $N(R)$ is similar in all silicates. However we do not know how to evaluate $N(R)$ for other minerals. Furthermore, a detailed model describing the annealing of extended defects in the high-temperature range is not available, and the variations of λ_c with the annealing temperature have still to be determined experimentally.

We will soon propose a track-formation mechanism intended to improve this situation, and which can be qualitatively outlined as follows. Each one of the extended defects represents the microscopic scar of an "ionization" spike. As the mean ionization potential is nearly constant in all silicates, the linear density of the spikes should be similar in these minerals. During the thermal spike, point defects formed by single-ionization spikes would quickly migrate towards the small clusters of defects generated by multiple ionization spikes which would thus act as "seeds" triggering the formation of the extended defects and their associated core zones. Consequently, in this two-step model, the value of λ_c should reflect not only the specific etching behavior of a mineral but also the spike-activated migration of defects in its structure. We are currently investigating how this qualitative picture can be improved by determining the critical ion fluences required to amorphize various silicates and the corresponding sputtering rates. Indeed, as first suggested by Seiberling *et al.*,[23] the sputtering

rate should be directly correlated to the average number of atoms initially set in motion in spikes occurring in the near vicinity of the surface. On the other hand, the amorphizing fluences would mostly reflect the much greater number of defects aggregated during the migration step of the track-formation mechanism.

The derived values of λ_c for krypton tracks in mica ($\lambda_c \sim 900$ Å) are much larger than the diameter (~20 Å) of the radiation-damaged core of fission fragment tracks in the same mineral, as inferred previously[2,6] from two distinct types of reliable etching experiments. It could thus be argued that our measurements of the λ_c values are in striking disagreement with previous measurements. However λ_c refers to the longitudinal and not to the lateral spread of the core zones, which are expected to be highly assymetrical in any concept of a track-forming spike mechanism.

Another difficulty arises from the well-known observation that lunar fossil Fe tracks anneal at a much higher temperature (~700 °C) than fresh Fe tracks, whereas they are already partially annealed (shorter total length). This apparent paradox can possibly be interpreted by noting that in solar flare cosmic rays, protons are ~10^4 times more abundant than Fe ions. The high densities of point defects induced by the protons in the grains could cluster around extended defects produced by Fe ions, which would thus enlarge their size and increase their thermal stability. Double irradiation experiments, involving high fluxes of protons before and/or after the Fe irradiation, are needed to test this hypothesis.

VI. CONCLUSION

Small-angle x-ray scattering experiments show that latent tracks produced by heavy ions in silicates consist of point defects and extended defects. The linear density of extended defects falls off much more rapidly with increasing residual ranges than the primary ionization rate. The track-etching model derived from these observations well accounts for the etching of tracks in mica and labradorite. In particular, the bimodal structure of the length distribution of partially annealed tracks in mica and the detailed variation of the etch rate along Fe and Kr tracks in labradorite are correctly predicted, using the same $N(R)$ distribution of extended defects for both minerals. Thus, the differences between the sensitivity of silicates arise mainly not from track registration, but from track revelation. Classical concepts such as the etching efficiency and the etchable range $\Delta R(Z)$ can be reevaluated in terms of our basic parameters, among which the effective length λ_c of the core zones plays a dominating role.

From this model we derived a few preliminary guidelines already used for improving the determination of the chemical abundance of very heavy cosmic-ray nuclei from etched-track studies in feldspars. These guidelines will be applied to other important applications of track studies in natural minerals in a forthcoming paper. However, these applications require a painstaking study of the specific etching behavior of minerals because we have not as yet a sufficient understanding of the track-formation mechanism.

[1]R. L. Fleischer, P. B. Price, R. M. Walker, and E. L. Hubbard, Phys. Rev. 133A, 1443 (1964).
[2]R. L. Fleischer, P. B. Price, and R. M. Walker, Annu. Rev. Nucl. Sci. 15, 1 (1965).
[3]P. B. Price, R. S. Rajan, and A. S. Tamhane, Astrophys. J. 151, L109 (1968).
[4]R. L. Fleischer and P. B. Price, J. Geophys. Res. 69, 331 (1964).
[5]P. B. Price, R. S. Rajan, and A. S. Tamhane, J. Geophys. Rev. 72, 1377 (1967).
[6]M. Maurette, Radiat. Eff. 3, 149 (1970).
[7]J. C. Dran, J. P. Duraud, and M. Maurette, Meteoritics 8, 347 (1973).
[8]E. Dartyge, J. P. Duraud, Y. Langevin, and M. Maurette, in *Proceedings of the Ninth Lunar Science Conference*, edited by R. D. Merrill (Pergamon, New York, 1978), Vol. 3, p. 2397.
[9]E. Dartyge, J. P. Duraud, and Y. Langevin, Radiat. Eff. 34, 77 (1978).
[10]P. B. Price, D. Lal, A. S. Tamhane, and V. P. Perelygin, Earth Planet. Sci. Lett. 19, 377 (1973).
[11]J. N. Goswami and D. Lal, in *Proceedings of the Sixth Lunar Science Conference*, edited by R. D. Merrill (Pergamon, New York, 1975), Vol. 3, 3541 (1975).
[12]R. L. Fleischer, P. B. Price, and R. M. Walker, *Nuclear Tracks in Solids* (University of California Press, Berkeley, 1975), p. 50.
[13]R. L. Fleischer, P. B. Price, and R. M. Walker, J. Appl. Phys. 36, 3645 (1965).
[14]J. C. Dran, J. P. Duraud, and M. Maurette, in *Proceedings of the Symposium No. 47, The Moon*, edited by H. Urey and S. K. Runcorn (D. Reidel, Dordrecht, Netherlands, 1972), p. 309.
[15]R. P. Henke and E. V. Benton, U. S. Naval Radiological Defense Laboratory Report No. TR-1102, 1966 (unpublished).
[16]M. Lambert, A. M. Levelut, M. Maurette, and H. H H. Heckmann, Radiat. Eff. 3, 155 (1970).
[17]E. Dartyge, Ph.D. thesis, Université Paris XI, 1979 (unpublished).
[18]R. Katz and E. J. Kobetich, Phys. Rev. 170, 401 (1968).
[19]R. L. Fleischer, in press.

[20]D. Lal, Space Sci. Rev. 9, 623 (1969).
[21]D. E. Yuhas, R. M. Walker, H. Reeves, G. Poupeau, P. Pellas, J. C. Lorin, G. C. Chetrit, J. L. Berdot, P. B. Price, I. D. Hutcheon, H. H. Hart, R. L. Fleischer, G. M. Comstock, D. Lal, J. N. Goswami, and N. Bhandari, in *Proceedings of the Third Lunar Science Conference*, edited by D. R. Criswell (MIT Press, Cambridge, Mass., 1972), Vol. 3, p. 2941.
[22]D. Lal, A. V. Muralli, R. S. Rajan, A. S. Tamhane, J. C. Lorin, and P. Pellas, Earth Planet. Sci. Lett. 5, 111 (1968).
[23]L. E. Seiberling, J. E. Griffith, and T. A. Tombrello, in *Lunar and Planetary Science XI*, edited by the Lunar and Planetary Institute (LPI/USRA, Houston, 1980), p. 1021.